Dalton Transactions

PAPER

View Article Online
View Journal | View Issue

Cite this: *Dalton Trans.*, 2016, **45**, 1201

Formazanido complexes of heavier group 13 elements aluminium, gallium, and indium†

W. Schorn, D. Grosse-Hagenbrock, B. Oelkers‡ and J. Sundermeyer*

Received 6th October 2015,
Accepted 18th November 2015

DOI: 10.1039/c5dt03906a

www.rsc.org/dalton

The preparation, molecular structures and physical properties of novel heavy group 13 metal formazanido complexes are described. The trimethyl derivatives MMe_3 (M = Al, Ga, In) react with 1,3,5-triphenylformazan (Htpf) in a 1 : 1 ratio to give methane and metallacycles of the type [M(tpf)Me_2]. While [Al(tpf)Me_2] and [Ga(tpf)Me_2] are mononuclear compounds with six-membered rings and coordination number 4 in solution and in the crystalline state, indium derivative [In(tpf)Me_2] forms oligomers in non-coordinating solvents according to NMR studies, these are probably N-bridged dimers with coordination number 5 at indium. The oligomer is cleaved by addition of one equivalent of pyridine or 4-dimethylaminopyridine (DMAP). The complexes [M(tpf)Me_2] (M = Al, Ga) and [In(tpf)Me_2(DMAP)] are characterized by XRD analyses. They are unique examples of main group metal formazane ring systems of the third and higher periods. The UV-Vis solution spectra of the neutral ligand Htpf and its metallated compounds [M(tpf)Me_2] (M = Al, Ga, In) are discussed.

Introduction

Since the first description of 1,3,5-triphenylformazan (Htpf, **1**) in 1884 by Pinner,[1] formazans and complexes derived therefrom have become an interesting class of dyes and coloured organic ligands with a number of applications as coloured indicators for several metal ions.[2,3] The intrinsic redox chemistry of the ligand was used as a measure for seed germinability,[4] since colourless tetrazolium cations can be reduced to coloured formazans by vital tissues (Scheme 1).

Even more interesting redox behaviour was discovered in 1964 by Kuhn *et al.*[5] *N*-Methylation of formazans and subsequent oxidation resulted in the formation of so-called verdazyls (Scheme 2). These are air- and water-stable, purely organic radicals that can be isolated and stored over months without decomposition.[6]

More recently, it was discovered by the groups of Hicks, Otten and Gilroy,[7–9] that the unique stability of these nitrogen-rich radicals can also be observed in isoelectronically related boron compounds and borataverdazyl radical anions (Scheme 3).

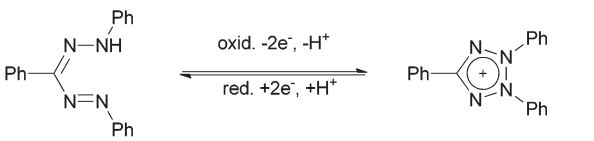

Scheme 1 Redox chemistry of formazans and tetrazolium cations.

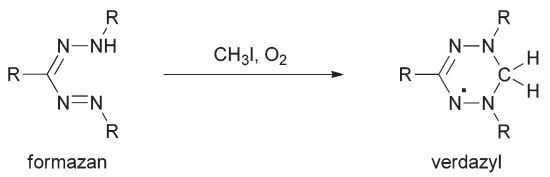

Scheme 2 Alkylation and oxidation of formazans yields verdazyls.

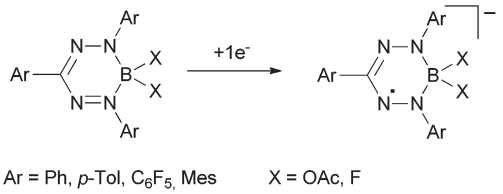

Scheme 3 Boron formazan complexes.[7–9]

Fachbereich Chemie der Philipps-Universität Marburg and Materials Science Center, Hans-Meerwein-Straße 4, 35307 Marburg, Hessen, Germany.
E-mail: jsu@staff.uni-marburg.de

†Electronic supplementary information (ESI) available: NMR spectra and details of the crystal structure analyses. CCDC 1414630–1414633. For ESI and crystallographic data in CIF or other electronic format see DOI: 10.1039/c5dt03906a

‡Current address: Fachbereich Chemie der TU Kaiserslautern, Erwin-Schrödinger-Straße 54, 67663 Kaiserslautern, Germany.

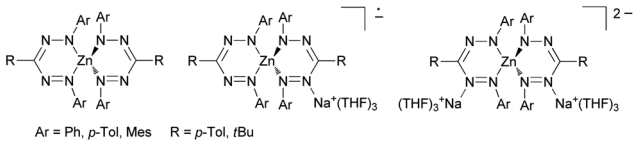

Scheme 4 Redoxactive zinc formazanido complexes.[19]

In sharp contrast the coordination chemistry of these formazanes and anionic formazanido ligands towards transition metals has a long-standing tradition following pioneering work of Bamberger *et al.*[10] However, despite of a variety of methods available for their synthesis,[1,11–14] formazan complexes typically have been limited to *N*,*N*-diaryl ligands. Recently their transition metal chemistry has experienced a renaissance arising from the insight that formazanido ligands are aza-analogues of most prominent β-ketiminato(1−) ligands.[15,16] However, in sharp contrast to β-ketiminato(1−) ligands, the non-innocent formazanido(1−) ligand can be reversibly reduced to the complex-stabilized radical dianionic (2−) state, *e.g.*, in the zinc complex shown in Scheme 4.[7,17–20]

Next to the abovementioned boron compounds, the only other well characterized main group element formazanido complexes described so far are some structurally characterized alkali metal formazanides.[21] In this paper, we describe the first formazanido(1−) compounds of the three heavier group 13 elements aluminium, gallium and indium.

Results and discussion

We realized that triphenyl formazane (Htpf, **1**) reacts selectively with trimethyl alane, gallane and indane under elimination of methane. The isolated products gave elemental analyses and HR-EI mass spectra in accord with the sum formula $C_{21}H_{21}MN_4$ (M = Al (**2**), Ga (**3**), In (**4**)) (Scheme 5).

In the ^{1}H NMR spectra of **2–4** the absence of any N–H protons of the neutral ligand is observed. The integral ratios clearly give evidence of the presence of a deprotonated ligand moiety and one dimethyl fragment MMe_2 (M = Al, Ga, In).

The NMR spectra of **2** and **3** show signal patterns that match the expected spectra for C_2- or C_s-symmetric compounds: one signal for both MMe_2 groups (M = Al, Ga) as well as the magnetic equivalence of the two peripheral *N*-phenyl rings lead to the assumption that **2** and **3** exist as six-membered MN_4C rings with tetrahedrally coordinated Al^{3+} and Ga^{3+} in solution. This corresponds to the structure in the crystalline state (see XRD analysis below). No further reaction of **2** and **3** with excess **1** was observed in hot toluene, a consequence of steric and electronic saturation by the set of donor ligands.

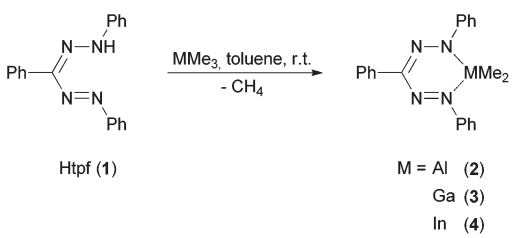

Scheme 5 Synthesis of group 13 formazanido complexes.

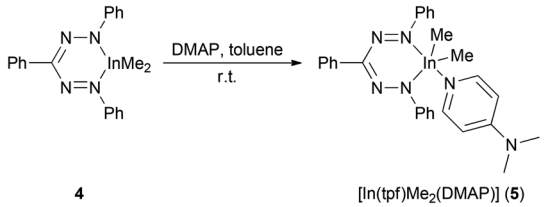

Scheme 6 Preparation of the DMAP adduct **5**.

The NMR spectra of indium complex **4** differ from the aforementioned ones: two methyl signals for the $InMe_2$ moiety and three magnetically non-equivalent phenyl rings are observed in C_6D_6. This can be explained by the fact that due to the much larger ionic radius of In^{3+} (80 pm) compared to Al^{3+} (53.3 pm) and Ga^{3+} (62 pm) [In(tpf)Me_2] forms dimers or oligomers in non-coordinating solvents.[22] This is most likely accomplished by bridging metallated N-atoms, as these are the most nucleophilic donors. This in turn would lead to coordination number five at indium, formation of a In_2N_2 core and loss of C_2- or C_s-symmetry in non-coordinating solvents. In accord with this assumption, addition of three-molar excess [D_5]-pyridine to the NMR sample of **4** in C_6D_6 resulted in the observation of only one set of methyl and *N*-phenyl protons at 25 °C similar to the spectra of **2** and **3**. This is most likely a result of pyridine coordination and dimer/oligomer dissociation. While the isolated DMAP complex **5** shows no symmetry in the solid state and solution (see below), it is proposed that **4** + [D_5]-pyridine undergoes rapid ligand exchange of coordinated and free pyridine with two exchanging pyridine coordination sites. In order to get more insight into this exchange process, a ^{1}H-NMR spectrum was recorded at the low temperature limit: at −60 °C the resulting spectrum of **4** + [D_5]-pyridine shows a clear splitting of the methyl signal, which is explained by slowing down the ligand exchange on the NMR time scale.

In order to gain final insight into the metal configuration involved in pyridine adducts, the strong donor 4-dimethylaminopyridine (DMAP) was added to **4** in toluene yielding [In(tpf)Me_2(DMAP)] (**5**) as a microcrystalline deep blue compound (Scheme 6). The isolated complex **5** reveals two signals δ_{In-Me} at room temperature and at −60 °C in CD_2Cl_2. This implies, that there is no plane of symmetry and no ligand exchange in the molecule in CD_2Cl_2 solution. This would be explainable *e.g.* by a non planar InN_4C ring in case of a trigonal bipyramidal or tetragonal pyramidal indium complex (see below, result of the solid state structure).

UV-Vis spectra of the complexes and neutral ligand

UV-Vis spectra of the compounds **1–5** were recorded in hexane.

Spectra of **1–3** in hexane are shown in Fig. 1.

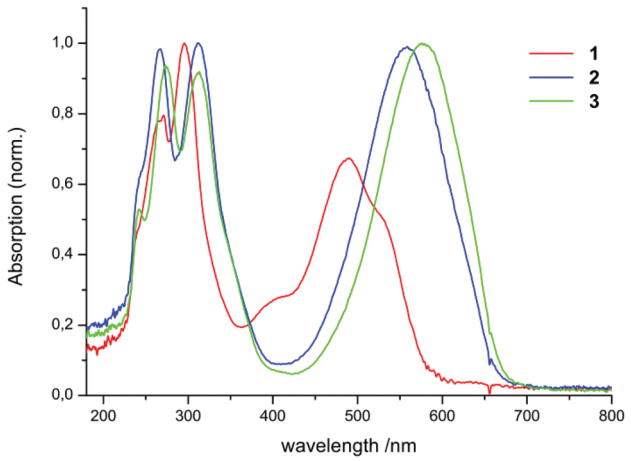

Fig. 1 UV-Vis spectra of the compounds **1–3** in hexane.

The complexes **2**, **3**, **4**, and **5** dissolve with a blue colour in hexane, while **1** is red in solution. The spectra of **1**, **2**, and **3** show two distinct absorption regions: the first one lies in the UV region (**1**: 240–330 nm, **2**: 240–340 nm, **3**: 240–340 nm). This absorption can be explained by the excitation of the phenyl moieties of the ligand. The second one lies in the visible range (**1**: 450–540 nm, **2**: 490–620 nm, **3**: 510–640 nm). One interesting feature in the spectrum of **1** is the appearance of an additional weak band at 400 nm. This can be attributed to the absorption of the *E*,s-*cis*,*E* isomer of the neutral ligand **1**. Hausser *et al.* could show[14,23] that exposing formazan solutions to light (λ < 480 nm) leads to a colour change from red to yellow along with a shift of the absorption maximum from about 490 to 400 nm. This colour change is due to the photo-induced isomerization of one of the double bonds within the ligand backbone.

Since the ratio of the intensities between the maximum at 400 nm and the remaining maxima varied during the measurements, no extinction coefficient was determined for **1**. All absorption maxima and extinction coefficients are listed in Table 1.

The spectra of **4** and **5** are more complicated. The most obvious reason is partial hydrolysis accompanying the dissolution of these extremely oxygen- and water-sensitive indium compounds at a sufficiently low molar concentration needed for UV-Vis measurements of compounds with such high extinction coefficients. The water content of *n*-hexane was checked to be <10 ppm.[24] Nevertheless partial hydrolysis during the UV-Vis sample preparation and recording is indicated by the appearance of overlapping bands of Htpf **1** (Fig. 2). Two of the maxima of extreemly diluted **4** and **5** are identical with the spectrum of Htpf. A weak absorption at about 400 nm is characteristic for the aforementioned presence of the *E*,s-*cis*,*E* isomer of the neutral ligand. Therefore the absorption maxima for **4** in Table 1 are estimated values obtained by substracting the spectrum of pure **1** from the mixture of **4** and **1** (Fig. 2). Under these conditions it seems unappropriate to calculate extinction coefficients for **4**. NMR samples of **4** or **5** recorded at higher concentration did not indicate any free ligand **1**.

The determined absorption maxima and extinction coefficients are in agreement with reports of Berry *et al.*[6] and Gilroy *et al.*[12,25] They attribute the red shift of the complexes compared to the protonated neutral formazans to the fixed conformation and the anionic character of the ligand moiety. The comparison of our studies with a literature known boron complex shows that the higher aluminium, gallium, and indium analogues (**2**, **3**, and **4**, respectively) absorb increasingly more red-shifted (Scheme 7).

This can be explained with an increasingly anionic character of the ligand moiety going from boron to indium. Interestingly, the extinction coefficient of the boron complex lies considerably below its higher homologues aluminium and gallium. We plan to further investigate this trend by evaluation of HOMO and LUMO energies by a combined CV and theoretical study. A preliminary CV screening on **2–4** indicates irreversible redox processes that might be attributed to follow-up reactions of the labile radical metal alkyls. Therefore we are planning to apply electrochemically more robust metal ligands in this chemistry.

Table 1 UV-Vis spectroscopic data for **1–4**

Substance	Absorption maximum/nm	Extinction coefficient/ (L mol^{-1} cm^{-1})
Htpf (**1**)	271, 295, 400, 490	Not determined, see above
[Al(tpf)Me$_2$] (**2**)	267	16 550 (±130)
	312	16 830 (±70)
	559	16 210 (±270)
[Ga(tpf)Me$_2$] (**3**)	242	11 370 (±440)
	274	20 860 (±360)
	313	19 960 (±180)
	576	20 960 (±200)
[In(tpf)Me$_2$] (**4**)	243, 279, 314, 591[a]	Not determined, see below

[a] Estimated values from difference spectra of **1** and mixture (**1** + **4**).

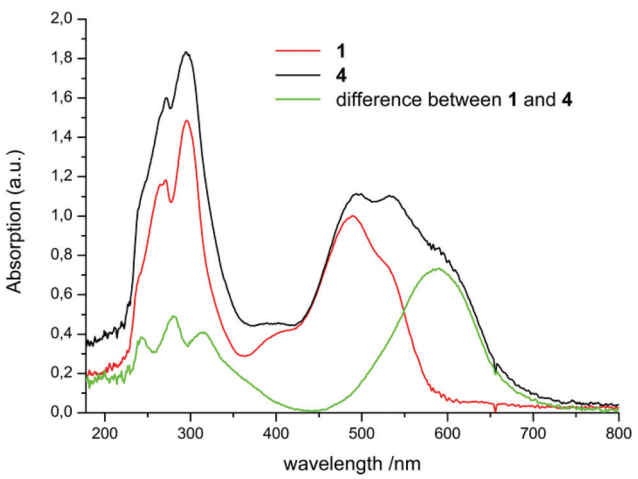

Fig. 2 UV-Vis spectra of **1** and **4** in hexane.

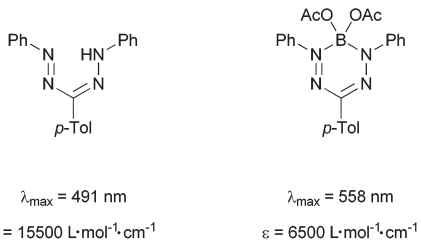

Scheme 7 Extinction coefficients and absorption maxima of formazans and formazan complexes prepared by Berry *et al.*[6]

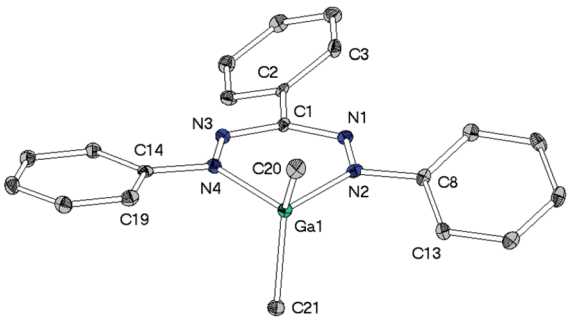

Fig. 4 Molecular structure of [Ga(tpf)Me_2] (**3**), hydrogen atoms have been omitted for clarity. Selected bond lengths/Å: Ga1–C20 1.966(3), Ga1–C21 1.961(3), Ga1–N2 2.001(2), Ga1–N4 2.010(2), C1–N1 1.346(3), C1–N3 1.343(4), N1–N2 1.306(3), N2–N4 2.813(3), N3–N4 1.313(3). Selected angles/°: C20–Ga1–C21 121.6(1), C20–Ga1–N2 107.4(1), C20–Ga1–N4 113.8(1), C21–Ga1–N2 112.5(1), C21–Ga1–N4 107.8(1), N2–Ga1–N4 89.1(1), Ga1–N2–C8–C13 26.2(3), Ga1–N4–C14–C19 9.7(3), C1–N1–N2–C8 1.2(2), C1–N3–N4–C14 1.9(2), C3–C2–C1–N1 26.9(4).

Crystal structures of Htfp (1), [Al(tpf)Me_2] (2), [Ga(tpf)Me_2] (3), and [In(tpf)Me_2(DMAP)] (5)

As a fundament for further theoretical studies the molecular structures of aluminium, gallium and indium complexes **2**, **3**, and **5** were determined by single crystal XRD analyses.

Crystal structure of 1. Compound **1** was crystallized at room temperature by layering a toluene solution with hexane. **1** crystallizes in the monoclinic space group $P2_1$ (Table S1, ESI†). The structure determination reveals a virtually perfectly planar 6-membered ring with the acidic proton in an asymmetric bridging position between both peripheral N atoms, very similar to the related molecular structure described by Gilroy *et al.*[7] with a *p*-tolyl substituent in the central position (further details see Fig. S9 ESI†).

Crystal structures of 2 and 3. Compounds **2** and **3** were crystallized by cooling a hexane solution to −23 °C. Both complexes are isostructural and crystallize in the orthorhombic space group *Pcan* with eight molecular units per unit cell. The molecular structures (Fig. 3 and 4) reveal a distorted tetrahedral coordination at the cations Al^{3+} and Ga^{3+}. Two binding sites are occupied by the outer nitrogen atoms of the deprotonated ligand and the coordination sphere is completed by two methyl moieties. The metal–carbon bond lengths (**2**: 1.960(2)/1.952(3) Å; **3**: 1.966(3)/1.962(3) Å) as well as the metal–nitrogen bond lengths (**2**: 1.937(2)/1.951(2) Å; **3**: 2.001(2)/2.010(2) Å) are in the range of known [M(N–N)Me_2] (M = Al, Ga) strucural motifs (Scheme 8).[26,27]

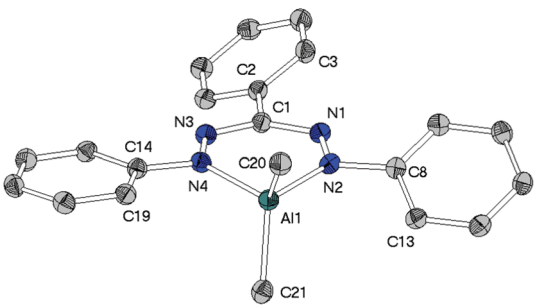

Fig. 3 Molecular structure of [Al(tpf)Me_2] (**2**), hydrogen atoms have been omitted for clarity. Selected bond lengths/Å: Al1–C20 1.960(2), Al1–C21 1.952(3), Al1–N2 1.937(2), Al1–N4 1.951(2), C1–N1 1.349(3), C1–N3 1.340(3), N1–N2 1.317(2), N2–N4 2.765(2), N3–N4 1.315(2). Selected angles/°: C20–Al1–C21 117.0(1), C20–Al1–N2 108.8(1), C20–Al1–N4 114.6(1), C21–Al1–N2 113.8(1), C21–Al1–N4 109.0(1), N2–Al1–N4 90.7(1), Al1–N2–C8–C13 27.0(3), Al1–N4–C14–C19 8.9(3), C1–N1–N2–C8 1.5(2), C1–N3–N4–C14 2.0(2), C3–C2–C1–N1 26.6(3).

The heterocycles MN_4C are nearly planar as shown by the sum of angles within these 6-membered cycles (**2**: 719.2(4)°, **3**: 719.1(6)°). This planarity allows the methyl groups to avoid each other's steric demand leading to the widening of the angles CH_3–M–CH_3 (**2**: 117.0(1)°, **3**: 121.6(1)°), which clearly deviate from the ideal tetrahedral angle of 109.5°.

While in neutral ligand Htpf **1** all three phenyl groups are coplanar to the inner HNNCNN ring, phenyl groups of **2** and **3** show no preference for a particular conformation: their torsion angles with respect to the ligand plane range from 9° to 28°. This difference is most likely due to steric repulsion between the *ortho*-protons of the peripheral phenyl substituents and the methyl groups of the MMe_2-moiety.

Crystal structure of 5. **5** was crystallized by layering a toluene solution with hexane at room temperature. [In(tpf)Me_2(DMAP)] crystallizes in the monoclinic space group $P2_1/c$ with four molecules in the unit cell (Fig. 5).

The indium coordination is inbetween the limits of a distorted square pyramid and a trigonal bipyramid: describing it in the latter configuration, the peripheral nitrogen atoms of the triphenylformazanido ligand occupy one apical and one equatorial position, whereas the DMAP ligand is bound *via* the other apical coordination site. The two remaining equatorial

Scheme 8 Examples of tetrahedral complexes of the type.[26,27]

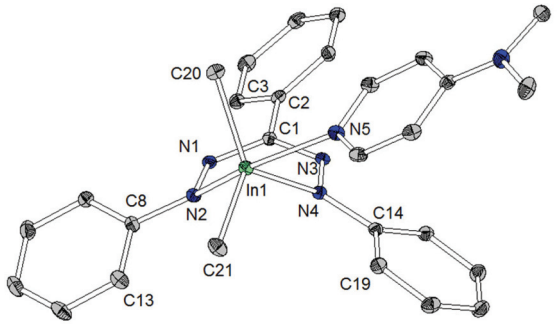

Fig. 5 Molecular structure of [In(tpf)Me_2(DMAP)] (**5**), hydrogen atoms have been omitted for clarity. Selected bond lengths/Å: In1–C20 2.153(2), In1–C21 2.155(2), In1–N2 2.451(1), In1–N4 2.269(1), In1–N5 2.369(1), C1–N1 1.356(2), C1–N3 1.339(2), N1–N2 1.293(2), N2–N4 2.703(2), N3–N4 1.322(2). Selected angles/°: C20–In1–C21 137.7(1), C20–In1–N2 86.7(1), C20–In1–N4 107.3(1), C20–In1–N5 91.4(1), C21–In1–N2 101.3(1), C21–In1–N4 114.4(1), C21–In1–N5 100.0(1), N2–In1–N4 69.7(1), N2–In1–N5 150.1(1), N4–In1–N5 82.5(1), In1–N2–C8–C13 50.9(2), In1–N4–C14–C19 16.0(2), C1–N1–N2–C8 9.8(1), C1–N3–N4–C14 21.2(1), C3–C2–C1–N1 21.5(2).

sites are occupied by two methyl groups. The indium–carbon bond lengths (2.153(2)/2.155(2) Å) show no significant difference to related complexes (Scheme 9).[28,29]

The shortest In–N distance of the formazan ligand is observed in the equatorial plane (In1–N4: 2.269(1) Å), indicating a localized amide character, while a longer In–N distance (In1–N5: 2.368(1) Å) is found towards the apical DMAP ligand and the longest one (In1–N2: 2.450(1) Å) corresponds to the (formally) neutral diazene –N=NPh donor *trans* to DMAP. This points out that the equivalence of both N-donor centers of tpf as observed for **2** and **3** is suspended upon coordination of DMAP by increasing the coordination number.

There are some further structural differences between **5** and the lighter homologues **2** and **3**. In contrast to the aluminium and gallium complex the metallacycle in **5** shows a considerable deviation from planarity: the angle between the planes N1–N2–N3–N4 and N2–In1–N4 amounts to 130.9(1)° in **5** (**2**: 173.9(1)°, **3**: 173.8(1)°). Thus the tpf complex **5** shows a deviation from ring planarity comparable with the doming of very large metal ions in porphyrins and phthalocyanins.[30] This is due to the larger In^{3+} cation and the larger coordination number caused by the co-ligand DMAP, which pulls the cation out of the ligand plane.

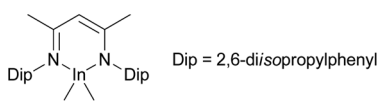

Dip = 2,6-di*iso*propylphenyl

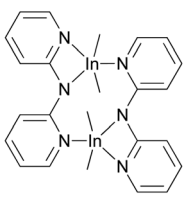

In-C: 2.148(1)/2.168(1) Å In-N: 1.190(1)/2.204(1) Å

In-C (av): 2.142 Å

Scheme 9 Examples of dimethylindium complexes.[28,29]

Conclusions

Novel formazanido complexes of the higher group 13 elements Al, Ga and In are described. The complexes were fully characterized by NMR, IR, and UV-Vis spectroscopy as well as by combustion analyses, high resolution EI mass spectrometry, and crystal structure analyses. Thus these complexes represent the first structurally characterized formazanido main group metal complexes with the exception of a few alkali metal complexes and metalloid boron complexes. The compounds contain reactive metal carbon bonds suitable for further reactivity studies. Their UV-Vis spectra in hexane show a red shift compared to the neutral ligand 1,3,5-triphenylformazan which can be attributed to the anionic charge within the ligand of the complexes leading to a energetically higher HOMO and a larger HOMO–LUMO gap. This assumption will be further evaluated by a combined CV and DFT study including *N*,*N*-dialkyl formazanes and more robust non-alkyl metal complexes.

Experimental

Materials and methods

All reactions were carried out under inert atmosphere using standard Schlenk techniques. Moisture and air sensitive substances were stored in a conventional nitrogen-flushed glovebox. The utilized solvents as well as deuterated solvents were distilled under nitrogen from an appropriate drying agent (hexane, toluene, THF, C_6D_6: Na/K) and stored under nitrogen over molecular sieves (4 Å). Commercially available 1,3,5-triphenylformazan (Htpf, >90%, Sigma-Aldrich) was recrystallized from a 2 : 1 mixture of dry hexane/toluene. 4-Dimethylaminopyridine (DMAP) was used as obtained (Sigma-Aldrich). $AlMe_3$, $GaMe_3$ and $InMe_3$ were condensed from commercially available MOVPE bubblers and destilled before use. Spectra were recorded on the following spectrometers: NMR: Bruker AC300, Bruker DRX400, and Bruker DRX500; IR: Bruker Alpha ATR-IR; EI-MS: Finnigan MAT95; UV-Vis: Avantes AvaSpec-2048, Varian Cary-5000. Elemental analysis were performed on an Elementar Vario-Micro-Cube.

[Al(tpf)Me_2] (2). 0.61 g of **1** (2.03 mmol, 1.0 eq.) were dissolved in 15 mL of toluene. 0.16 g of $AlMe_3$ (2.22 mmol, 1.1 eq.) dissolved in 10 mL of toluene were added to the cherry-red formazan solution at room temperature. After a few minutes the color of the solution changed from cherry-red to deep blue and gas evolution could be observed. The reaction mixture was stirred overnight at room temperature. The solvent was removed *in vacuo*, 20 mL of hexane were added to the remaining viscous solid and the mixture was stirred for 2 h at room temperature. Afterwards the blue solution was filtered through a bed of Celite™, the filter cake was extracted with hexane (3 × 5 mL) and the filtrate was taken to dryness *in vacuo*. 0.65 g (1.82 mmol, 90%) of a deep blue solid were isolated. ^{1}H NMR (C_6D_6, 300 MHz): δ = −0.25 (s, 6 H, AlMe_2),

6.92–7.02 (m, 2 H, NPh(*para*)), 7.02–7.12 (m, 4 H, NPh(*meta*)), 7.17–7.27 (m, 1 H, CPh(*para*)), 7.27–7.37 (m, 2 H, CPh(*meta*)), 7.61–7.71 (m, 4 H, NPh(*ortho*)), 8.19–8.29 (m, 2 H, CPh(*ortho*)) ppm. $^{13}C\{^1H\}$ NMR (C_6D_6, 75 MHz): δ = −9.4 (Al*Me*$_2$), 122.1 (NPh(*ortho*)), 126.0 (CPh(*ortho*)), 128.4 (NPh(*para*)), 128.5 (CPh-(*para*)), 128.8 (CPh(*meta*)), 129.4 (NPh(*meta*)), 137.5 (N*C*N), 149.2 (NNC-C_{quart}), 150.0 (NN-C_{quart}) ppm. Anal. calc. for $C_{21}H_{21}AlN_4$: C, 70.77; H, 5.94; N, 15.72%. Found C, 70.39; H, 5.59; N, 15.52%. HR EI-MS:calc. for M^+ *m*/*z* 356.1582, obs. 356.1564. IR (neat, cm^{-1}): 3059, 3025, 2928, 2890, 1584, 1483, 1275, 1231, 1195, 750, 672, 647, 511.

[Ga(tpf)Me$_2$] (3). 0.61 g of **1** (2.03 mmol, 1.0 eq.) were dissolved in 15 mL of toluene. 0.27 g of $GaMe_3$ (2.35 mmol, 1.2 eq.) dissolved in 10 mL of toluene were added to the cherry-red formazan solution at room temperature. After a few minutes the color of the solution changed from cherry-red to deep blue and gas evolution could be observed. The reaction mixture was stirred overnight at room temperature. The solvent was removed *in vacuo*, 20 mL of hexane were added to the remaining viscous solid and the mixture was stirred for 2 h at room temperature. Afterwards the blue solution was filtered through a bed of Celite™, the filter cake was extracted with hexane (3 × 5 mL) and the filtrate was taken to dryness *in vacuo*. 0.69 g (1.73 mmol, 85%) of a deep blue solid were isolated. ^1H NMR (C_6D_6, 300 MHz): δ = 0.02 (s, 6 H, Ga*Me*$_2$), 6.93–7.03 (m, 2 H, NPh(*para*)), 7.04–7.14 (m, 4 H, NPh(*meta*)), 7.18–7.28 (m, 1 H, CPh(*para*)), 7.30–7.40 (m, 2 H, CPh(*meta*)), 7.55–7.65 (m, 4 H, NPh(*ortho*)), 8.23–8.33 (m, 2 H, CPh(*ortho*)) ppm. $^{13}C\{^1H\}$ NMR (C_6D_6, 75 MHz): δ = −6.7 (Ga*Me*$_2$), 121.7 (NPh(*ortho*)), 125.7 (CPh(*ortho*)), 128.00 (NPh(*para*)), 128.04 (CPh(*para*)), 128.8 (CPh(*meta*)), 129.4 (NPh(*meta*)), 138.5 (N*C*N), 147.4 (NNC-C_{quart}), 150.6 (NN-C_{quart}) ppm. Anal. calc. for $C_{21}H_{21}GaN_4$: C, 63.19; H, 5.30; N: 14.04%. Found C, 62.99; H, 5.35; N, 13.95%. EI-MS, exact mass (calc. for M^+) *m*/*z* 398.1022, (obs.) 198.1016. IR (neat, cm^{-1}): 3057, 3025, 2928, 2890, 1584, 1483 1353 1483, 1275, 1230, 1195, 750, 672, 647, 533 511.

[In(tpf)Me$_2$] (4). 0.60 g of **1** (2.00 mmol, 1.0 eq.) were dissolved in 20 mL of toluene. 0.35 g of $InMe_3$ (2.19 mmol, 1.1 eq.) dissolved in 10 mL of toluene were added to the cherry-red formazan solution at room temperature. After a few minutes the color of the solution changed from cherry-red to deep blue and gas evolution could be observed. The reaction mixture was stirred overnight at room temperature. The solvent was removed *in vacuo*, 20 mL of hexane were added to the remaining viscous solid and the mixture was stirred for 2 h at room temperature. Afterwards the blue solution was filtered through a bed of Celite™, the filter cake was extracted with hexane (3 × 5 mL) and the filtrate was taken to dryness *in vacuo*. 0.62 g of a deep blue solid (1.40 mmol, 70%) were collected. ^1H NMR (C_6D_6, 300 MHz): δ = −0.18 (s, 2.5 H, In*Me*$_2$), −0.03 (s, 3.5 H, In*Me*$_2$), 6.91–7.23 (m, 8 H, NPh(*meta*), NPh(*ortho*)), 7.35–7.38 (m, 2 H, NPh(*para*)), 7.50–7.57 (m, 3 H, CPh(*para*), CPh(*meta*)), 8.32–8.39 (m, 2 H, CPh(*ortho*)) ppm. Anal. calc. for $C_{21}H_{21}InN_4$: C, 56.78; H, 4.76; N, 12.61%. Found C, 56.71; H, 4.74; N, 12.63%. HR EI-MS: calc. for M^+ *m*/*z* 444.0805, obs. 444.0811. IR (neat, cm^{-1}): 3062, 3004, 2917, 1593, 1479, 1272, 1239, 1188, 1161, 754, 663, 597.

[In(tpf)Me$_2$(DMAP)] (5). 0.88 g of **4** (2.00 mmol, 1.0 eq.) and 0.24 g of DMAP (2.00 mmol, 1.0 eq.) were placed in a Schlenk tube and 20 mL of toluene were added. The blue solution was treated with ultra sound for 10 minutes. Afterwards the solvent was stripped off *in vacuo* and 20 mL of hexane were added. The blue suspension was filtered and the remaining solid was washed with a few portions of hexane. After drying of the remaining deep blue solid, 1.02 g (1.80 mmol, 90%) of the product were isolated.

^1H NMR (CD_2Cl_2, 300 MHz): δ = −0.03 (s, 6 H, In*Me*$_2$), 2.96 (s, 6 H, N*Me*$_2$), 6.42–6.44 (m, 2 H, InPy(*meta*)), 7.18–7.23 (m, 2 H, NPh(*para*)), 7.31–7.46 (m, 4 H, NPh(*meta*)), (m, 1 H, CPh(*para*)), (m, 2 H, CPh(*meta*)), 7.54–7.57 (m, 4 H, NPh(*ortho*)), 7.99–8.00 (m, 1 H, InPy(*ortho*)), 8.02 (m, 2 H, CPh(*ortho*)), 8.04–8.05 (m, 1 H, InPy(*ortho*)) ppm. Vt-^1H NMR (CD_2Cl_2, 300 MHz, 213 K): δ = −0.24 (s, 2 H, In*Me*$_2$), −0.12 (s, 4 H, In*Me*$_2$) 2.88 (s, 6 H, N*Me*$_2$), 6.28–6.29 (m, 2 H, InPy(*meta*)), 6.77–7.47 (m, 12 H, NPh(*para*), NPh(*meta*), (CPh(*meta*), NPh(*ortho*)), 7.60–7.62 (m, 2 H, CPh(*ortho*)), 7.72–7.74 (m, 2 H, InPy(*ortho*)), 8.05–8.06 (m, 1 H, CPh(*para*)) ppm. $^{13}C\{^1H\}$ NMR (CD_2Cl_2, 75 MHz): δ = −4.8 (Al*Me*$_2$), 39.3 (s, N*Me*$_2$) 107.0 (s, InPy(*meta*)), 120.9 (NPh(*ortho*)), 127.0 (s, CPh(*ortho*)), 127.1 (s, NPh(*para*)), 127.7 (CPh(*para*)), 128.5 (CPh(*meta*)), 129.7 (NPh(*meta*)), 129.9 (N*C*N), 149.3 (InPy(*ortho*)), 153.8 (NNC-C_{quart}), 154.9 (NN-C_{quart}) ppm. Anal. calc. for $C_{28}H_{31}InN_6$: C, 59.37; H, 5.52; N, 14.84%. Found C, 59.03; H, 5.43; N, 14.98%. IR (neat, cm^{-1}): 3062, 3031, 2968 2918, 1619, 1538, 1276, 1220, 1005, 802, 757, 475.

Single-crystal structure analyses

Crystallographic data are provided in Table 1 (ESI†). X-Ray data collection was performed *via* a Stoe IPDS II or Bruker D8 Quest area detector system using Mo-Kα radiation (λ = 71.073 pm). Stoe IPDS and Bruker SAINT software[31] was used for integration and data reduction. Structure solution and refinement was done with the WinGX program suite[32] using SIR92, SIR2004, SUPERFLIP and SHELX2014.[33]

For Htpf (**1**), the N–H proton H1 was located between the two nitrogen atoms N2 and N4. Within the accuracy of the measurement, no clear decision could be made as to whether a rather symmetric configuration or a superposition of two "normal" N–H···H configurations was present. As the former was the natural interpretation of the electron density map, it was arbitrarily chosen in this case.

Acknowledgements

This work was partly funded by DFG within GRK 1782. We thank the Crystallographic Service group, namely Dr K. Harms and associates, of the Fachbereich Chemie for XRD data collection.

References

1 A. Pinner, *Ber. Dtsch. Chem. Ges.*, 1884, **17**, 182.
2 A. G. Ciba, *CH* 246475, 1947.
3 R. M. Rush and J. H. Yoe, *Anal. Chem.*, 1954, **26**, 1345.
4 G. Lakon, *Plant Physiol.*, 1949, **24**, 389.
5 R. Kuhn and H. Trischmann, *Monatsh. Chem.*, 1964, **95**, 457.
6 (*a*) F. A. Neugebauer and R. Siegel, *Angew. Chem., Int. Ed. Engl.*, 1973, **85**, 485; (*b*) B. D. Koivisto and R. G. Hicks, *Coord. Chem. Rev.*, 2005, **249**, 2612; (*c*) D. E. Berry, R. G. Hicks and J. B. Gilroy, *J. Chem. Educ.*, 2009, **86**, 76.
7 J. B. Gilroy, M. J. Ferguson, R. McDonald, B. O. Patrick and R. G. Hicks, *Chem. Commun.*, 2007, 126.
8 M.-C. Chang and E. Otten, *Chem. Commun.*, 2014, **50**, 7431.
9 S. M. Barbon, J. T. Price, P. A. Reinkeluers and J. B. Gilroy, *Inorg. Chem.*, 2014, **53**, 10585.
10 E. Bamberger and E. Wheelright, *Ber. Dtsch. Chem. Ges.*, 1892, **25**, 3201.
11 H. von Pechmann, *Ber. Dtsch. Chem. Ges.*, 1892, **25**, 3175.
12 J. B. Gilroy, P. O. Otieno, M. J. Ferguson, R. McDonald and R. G. Hicks, *Inorg. Chem.*, 2008, **47**, 1279.
13 D. Jerchel and H. Fischer, *Justus Liebigs Ann. Chem.*, 1949, **563**, 200.
14 I. Hausser, D. Jerchel and R. Kuhn, *Chem. Ber.*, 1949, **82**, 515.
15 L. Bourget-Merle, M. F. Lappert and J. R. Severn, *Chem. Rev.*, 2002, **102**, 3031.
16 Y.-C. Tsai, *Coord. Chem. Rev.*, 2012, **256**, 722.
17 S. Hong, L. M. R. Hill, A. K. Gupta, B. D. Naab, J. B. Gilroy, R. G. Hicks, C. J. Cramer and W. B. Tolman, *Inorg. Chem.*, 2009, **48**, 4514.
18 J. B. Gilroy, M. J. Ferguson, R. McDonald and R. G. Hicks, *Inorg. Chim. Acta*, 2008, **361**, 3388.
19 M.-C. Chang, T. Daun, D. P. Day, M. Lutz, G. G. Wildgoose and E. Otten, *Angew. Chem., Int. Ed.*, 2014, **53**, 4118.
20 M.-C. Chang, P. Roewen, R. Travieso-Puente, M. Lutz and E. Otten, *Inorg. Chem.*, 2015, **54**, 379.
21 R. Travieso-Puente, M.-C. Chang and E. Otten, *Dalton Trans.*, 2014, **43**, 18035.
22 R. D. Shannon, *Acta Crystallogr., Sect. A: Cryst. Phys., Diffr., Theor. Gen. Cryst.*, 1976, **32**, 751.
23 I. Hausser, D. Jerchel and R. Kuhn, *Chem. Ber.*, 1949, **82**, 195.
24 The water contents of the solvents were determined by Karl Fischer titration: hexane 6.5 ppm, THF 8.9 ppm.
25 J. B. Gilroy, B. O. Patrick, R. McDonald and R. G. Hicks, *Inorg. Chem.*, 2008, **47**, 1287.
26 H. Gornitzka and D. Stalke, *Organometallics*, 1994, **13**, 4398.
27 D. Vidovic, J. N. Jones, J. A. Moore and A. H. Cowley, *Z. Anorg. Allg. Chem.*, 2005, **631**, 2888.
28 H. Gornitzka, *Eur. J. Inorg. Chem.*, 1998, **3**, 311.
29 M. Stender, B. E. Eichler, N. J. Hardman, P. P. Power, J. Prust, M. Noltemeyer and H. W. Roesky, *Inorg. Chem.*, 2001, **40**, 2794.
30 K. M. Kadish, K. M. Smith and R. Guilard, Academic Press, San Diego, *The porphyrin handbook*, 2000.
31 (*a*) *STOE X-AREA and X-RED*, Stoe & Cie GmbH, Darmstadt, Germany, 2001; (*b*) *Bruker SAINT*, Bruker AXS Inc., Madison, Wisconsin, USA, 2012.
32 L. J. Farrugia, *J. Appl. Crystallogr.*, 1999, **32**, 837.
33 (*a*) A. Altomare, G. Cascarano, C. Giacovazzo and A. Guagliardi, *J. Appl. Crystallogr.*, 1993, **26**, 343; (*b*) M. C. Burla, M. Camalli, B. Carrozzini, G. L. Cascarano, C. Giacovazzo, G. Polidori and R. Spagna, *J. Appl. Crystallogr.*, 2003, **36**, 1103; (*c*) L. Palatinus and G. Chapuis, *J. Appl. Crystallogr.*, 2007, **40**, 786; (*d*) G. M. Sheldrick, *Acta Crystallogr., Sect. C: Cryst. Struct. Commun.*, 2015, **71**, 3.